A study of thermo-elastic characteristics of the machine tool spindle

Aleksandar Zivkovic[1,*], *Milos* Knezev[1], *Milan* Zeljkovic[1], *Slobodan* Navalusic[1], and *Livia* Dana Beju[2]

[1]University of Novi Sad, Faculty of Technical Science, Trg D. Obradovica 6, Novi Sad 21000, Serbia
[2]University „Lucian Blaga“ of Sibiu, Department of Industrial Engineering and Menagment, 10, Victoriei Bd., Sibiu, 550024, România

Abstract. In order to avoid the failure of machine tools spindles in the real machining process due to an increase in temperature, it is essential to predict its thermal behavior in the designing phase. The characteristics of machine tools significantly depend on the thermal-elastic behavior of the spindle. These parameters directly affect the productivity and quality of machining operations. This paper presents a thermal - elastic model of the machine tool spindle which was based on the quasi-static model of bearings and the finite element (FE) model of the spindle shaft. Based on quasi-static model of bearings with angular contact, heat generated and thermal contact resistances (TCR) are determined for each position of the balls. The aforementioned constraints have been applied to the 3D FE model of the spindle which allowed for establishing non-stationary change of temperature and thermal deformation. In order to prove the efficacy of the proposed model, experimental measurements of spindle and bearing temperatures were done using thermocouples and thermal imager.

1 Introduction

The development of the technology for high speed machine tools manufacturing must be observed from the point of view of machine tools application. It is essential to first answer the question of whether the spindle is meant for high cutting force machining, or for high rotation speeds. Thus, in the case of the former, spindle stiffness is the more important characteristic, while for the latter the specific speed coefficient is important. Currently, spindle manufacturers offer a wide range of spindle solutions depending on the machine tool application area. Non-uniform temperature distribution causes elastic thermal deformation of the spindle shaft, resulting in workpiece geometric and shape errors. The goal towards which the majority of researchers are headed is the increase in machine tool accuracy. The errors affecting machine tool accuracy can be grouped into four categories: geometrical, kinematic, thermal, and the errors produced by the cutting forces. Thermal errors account for the 40 to 70 % of total machine tool errors [1-2]. Other than that, about 75 % of machined workpieces geometrical errors occur due to temperature influence [3].

There is a connection between spindle's thermal and elastic behavior. The rise in temperature of spindle units produces thermal expansion of bearing elements, which causes

* Corresponding author: acoz@uns.ac.rs

increase bearing preload and thermal deformation on the spindle shaft. In practical working conditions, due to production errors, mounting errors, and the thermal deformations of the spindle-bearing system bearing clearances are not uniform, which leads to position deviation between the outer ring and spindle shaft [4-6]. The above mentioned, it is essential to determine thermal sources, sinks, and temperature distribution of machine tool spindle, in order to reduce and compensate for the thermal deformation of both the spindle and the entire machine tool.

The mathematical modeling and experimental approach for predicting thermo-elastic behavior of the machine tool spindle for different values of rotation speed is proposed in this paper. The bearing quasi-static model and 3D FE model of the spindle are related to thermal analysis. Based on Jones-Harris quasi-static model [7] and Hertz's contact theory the deformation, contact load, contact angle, and preload of the bearings was determined. Thermal and elastic spindle models were developed by using the finite element method. The boundary conditions, such as heat generated on the bearings, the heat transfer coefficients, and thermal contact resistance (TCR) of the joint surface, bearing stiffness were applied to the FE thermal and elastic model of spindle. Finally, in order to determine the efficacy of the proposed model, experimental measurements of spindle and bearing temperatures were performed using the thermocouple, infra-red thermometer, and thermal imager.

2 The thermal model of the machine tool spindle

The bearing model and the FE model of the spindle are used to determine the influences of non-linear thermal effects on the thermal characteristics of spindle. The proposed model is applied in researching the spindle thermal characteristics with "O" bearing arrangement with different rotation speeds. Heat generated by bearings $H_{1(t)}$ i $H_{2(t)}$ is the main heat source that is considered in the paper and is shown in Figure 1. The conditions of heat transfer from the spindle and the boundary conditions of heat dissipation are also shown in Figure 1. In this model heat flow resistance due to lubrication between balls and raceways is not considered, due to the minimal amount of grease. Also, the heat radiation is neglected because the temperature difference during the spindle rotation is small.

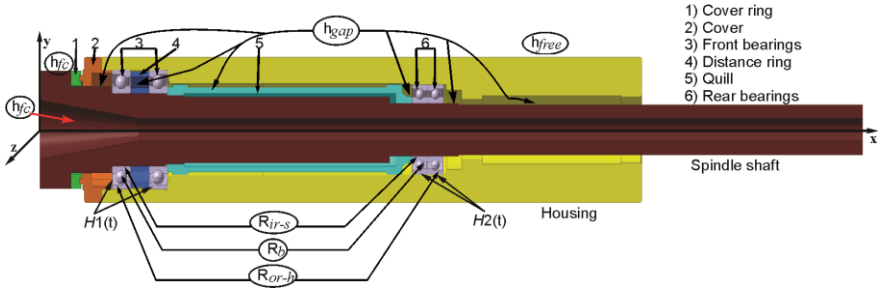

Fig. 1. Thermal model of the high spindle

2.1 Bearing model

The mechanical and thermal processes in the bearing are connected. As the speed of bearing rotation increases, so does the heat generated on the contact surfaces of the bearing. In the bearing model, three degrees of freedom are considered for the relative displacement of the inner raceways with compared to the outer raceways which is fixed. These consist of two linear displacements (δa, δr) and one rotation (θy), whereby, α_p is the contact angle of

the bearing ball after preload as it is shown on the Figure 2(a). The inertial forces affecting the balls causes the change of contact angles with the outer and inner raceways. Due to the change in contact angle with the raceways the line of action between the raceway groove curvature centers will not be collinear with the distance between centers A_N as depicted in Figure 2(a). Contact load and inertial loads acting on the ball are shown in Figure 2(b)

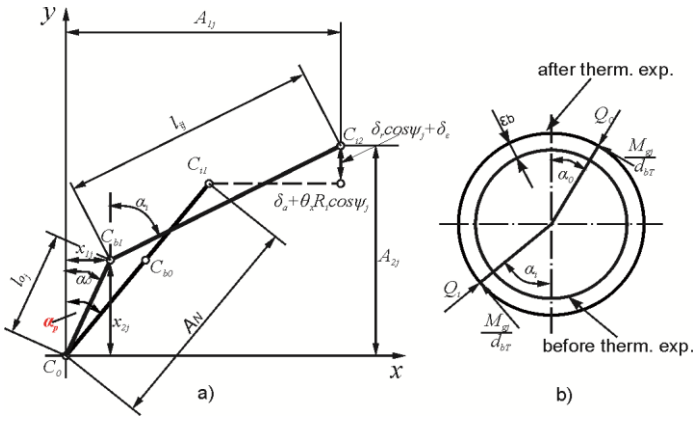

Fig. 2. (a) Position of raceway curvature centers, (b) Ball loading at angular position ψ_j

Contact angles with the outer and inner raceways are denoted by α_o and α_i respectively. The relation between local Hertz's contact forces $Q_{(j)}$ and deflection $\delta_{(j)}$ between ball and inner/outer raceway is defined as:

$$Q_{m,j} = K_m \delta_{m,j}^{3/2}; m = i,o; j = 1,2....Z \tag{1}$$

where *i, o* refer to inner and outer raceway, δ_m is deformation due to applied load. The previous relation is applicable when $\delta_{i(j)}>0$. Otherwise $Q_{oj}=F_{cj,}$ that is $\delta_{o,j}=(F_{cj}/K_o)^{2/3}$. The conditions in which the ball loses contact with the inner/outer raceways were based on [8] The determining of Hertz's contact stiffness Km (m=i,o) is based on [9] with the consideration of the change in bearing element dimension due to temperature increase.

After establishing the contact load and the contact angle, the radial and axial stiffness on the inner and outer raceway can be determined through Hertz's contact stiffness as:

$$\begin{aligned} k_{(i,o)xx} &= \left(1.5K_{(i,o)j}\delta_{(i,o)j}^{0.5}\right)\sin\alpha_{(i,o)j} \\ k_{(i,o)yy} &= \left(1.5K_{(i,o)j}\delta_{(i,o)j}^{0.5}\right)\cos\alpha_{(i,o)j} \end{aligned} \tag{2}$$

2.2 The heat generation of ball bearing

The generated heat of the bearing is created by three types of friction moment: torque due to applied load, torque due to viscosity of lubricant. Therefore, the friction torque due to applied load and due to viscosity of lubricant at each inner and outer contact with the raceway is formulated as:

$$M_{1m,j} = \left\{ f_1 \left(\frac{Q_{m,j}}{Q_{m(\max)}} \right)^{1/3} Q_{m,j} d_b + 10^{-7} f_0 \left(\nu_o n\right)^{2/3} {d_m}^3 \right\}; m = i,o \; j = 1,2...Z; \tag{3}$$

where there are: f_1 - bearing parameter dependent on the bearing type *;* $Q_{m(\max)}$ - maximum contact load; f_0 - a factor dependent on the type of bearing and method of lubrication; v_o - kinematic viscosity of the lubricant.

The heat generated in the contact zone for each ball is:

$$H_{m,j} = \omega_b M_{1m,j}; m = i, j; j = 1,2...Z \tag{5}$$

where the angular velocity of the ball (ω_b) is shown in paper [7].

2.2 Heat transfer model of the spindle

This paper presupposes that the mechanisms of heat transfer through the spindle are: the conduction between the balls and the raceways, the conduction between the outer ring and housing, the conduction between spindle shaft and the inner ring, convection in the annular gap, convection between the rotating body surface and the air and free convection of ambient air around the housing.

Conduction between balls and raceways The balls and rings are not made of the same material, and for those cases according to [10], thermal contact resistance for each ball is:

$$R_{b(m,j)} = \frac{1}{2\pi a_{m,j}\lambda_b}\psi\left(e,\frac{\pi}{2}\right) + \frac{1}{2\pi a_{m,j}\lambda_{ring}}\psi\left(e,\frac{\pi}{2}\right); m = i, o\ j = 1,2,....,Z \tag{6}$$

where λ_b and λ_{ring} are thermal conductivity of the balls and rings respectively, and $\psi(e,\pi/2)$ is a geometrical factor dependent on the size of contact area between balls and raceways.

Conduction between inner ring/spindle shaft and outer ring/housing Heat resistance *($R_{ir\text{-}s}$)* between the inner ring and the spindle shaft is determined by using the relation for cylinder heat resistance [11] :

$$R_{i,o} = \frac{\ln(R_{m(i,o)} / R_{n(i,o)})}{2\pi L_{l(i,o)} k} \tag{7}$$

where $R_{n(i,o)}$ and $R_{m(i,o)}$ are the inner and outer section radii which are observed in the inner or outer bearing ring, and $L_{(i)}$ is the length according to the inner section. Heat conductivity (λ) for steel is 46.6 W/m-K and it is valid for 20-200 °C.

Heat transfer from spindle Heat transfer coefficient for force convection can be established as [11]:

$$h_i = \frac{N_u \lambda_{air}}{d_j}; i = fc, gap; j = d, gap \tag{8}$$

where λ_{air} is the heat conductivity of air, N_u is Nusselt's number and d_j is the diameter of the flow cross-section of a tube. In case of annular gap of the spindle, d_j changes to the size of gap. For stationary surfaces such as the surface of the housing, free convection is considered, where the convection coefficient is taken from [12] and it is 13,5 W/(m^{2}K)

2.3 FE thermal and elastic model

In defining the thermal model of the spindle, the hexahedral element SOLID 90 was used to mesh solid structure. Model consists of 125353 solid elements and 211303 nodes in total. The finite elements CONTA174 and TARGET170 were used to simulate contact joints. To

simulate contact joints, contact pairs were created at the joints, and the real constant (TTC) was defined, i.e., the thermal contact conductivity for each ball, as well as for each contact between the outer ring/housing and inner ring/spindle shaft. Because of the spindle symmetry only a half of the three-dimensional model was considered, as shown in Fig. 15.

In modeling the elastic model of the spindle shaft, SOLID 186 element has been used, while the bearings have been modeled with spring-type finite element. The number of spring-type finite elements corresponds to the number of ball bearings in front and rear support. In Figure 15 is shown elastic model of the spindle shaft.

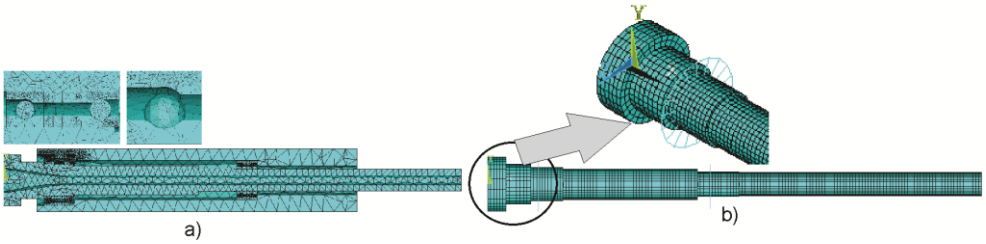

Fig. 3. FE spindle model: (a) *thermal*, (b) elastic.

3 Experimental setup

In order to validate simulation results, an experimental apparatus has been established to measure temperatures and displacement on the spindle nose shown in Fig. 4. The spindle is supported in the front with two bearings in a "0" arrangement (SKF 7011 CDGA/HC P4.), and in the rear with two bearings in a "0" arrangement (SKF 7008 CDGA/HC P4.). All the bearings are with lock-ring preload. To lubricate the bearing, the principle of minimal lubrication has been used, with the SKF LGLT 2 grease, which has a kinematic viscosity of 18 mm^2/s on 40 °C. The spindle is driven by motor, which has 9000 rpm maximum speed, through belt transmission. To measure the temperature of the spindle, thermocouples, infrared thermometer and thermal imager have been used. Non-contact inductive sensors B&K TR2 (6) have been used to measure displacement on the spindle nose, in vertical and horizontal plane.

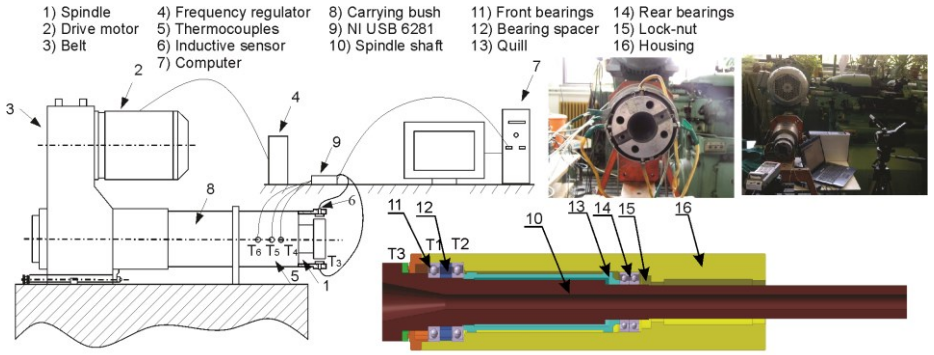

Fig. 4. A schematic of the experimental rig.

4 Results and Discussion

The analysis of thermo-elastic behavior of the spindle includes stationary and non-stationary temperature change and thermal deformation of the spindle nose, for different

rotation speeds. For the stationary and non-stationary analysis, the temperatures measured in different measuring points (Fig. 4) were compared to the predicted temperatures received from the mathematical model for different spindle speed.

Temperature analysis. Figure 5 shows the measured and simulated temperatures in 3 selected locations according to Figure 4 for different spindle speeds (1000 – 9000 rpm). These comparisons were applied to steady state solutions. The predicted temperatures of the outer rings of the front bearing, the housing near the front bearing, and of the spindle nose, match those that were measured for all tested spindle speeds. The maximum difference from 1.5 to 3 °C in stationary state, depending on the number of revolutions and measure location, is acceptable.

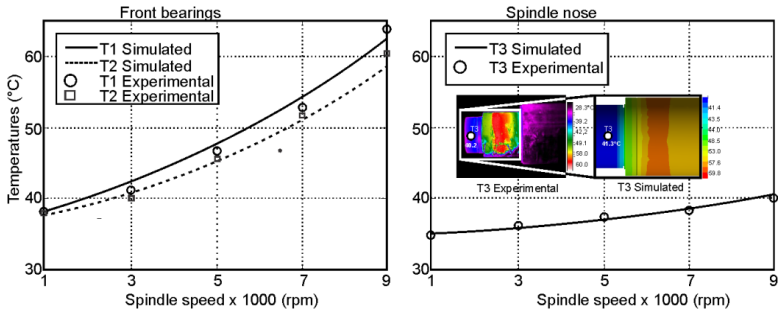

Fig. 5. Comparison temperatures in the steady state: a) front bearings; b) spindle nose.

In Fig. 6 (a) and (b) the change in temperature of the housing and spindle shaft is shown, respectively. These figures show invaluable information for determining axial thermal expansion and thermal flux. Based on the temperatures in previous figures, spindle construction can be improved by examining the conditions such as: cooling, lubrication, and bearing preload. Due to the temperature field distribution on the axis of symmetry, which easily produces thermal deformations, the result can be a larger thermal error and reduced machining accuracy. Therefore, some cooling measures can be taken so that the design structure is improved.

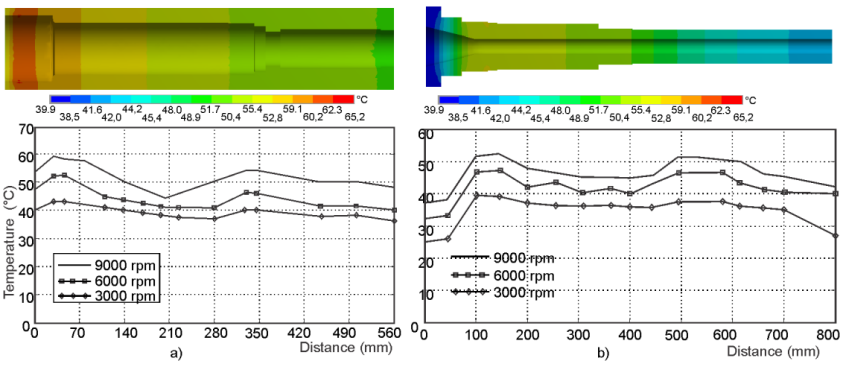

Fig. 6. The variation of temperature along axial direction (a) on the housing, (b) on the spindle shaft.

In Fig. 7 (a) and (b) there is a comparison between the simulated and the temperatures measured by thermal imager. The temperatures of the front bearings from the very start rise sharply at the early stage, and then gradually increase until reaching the final temperature, when the amount of heat generation is in balance with the heat dissipation into the ambient air. It takes about 60 min for the front bearings to reach a thermal equilibrium state. In fact, the rotational speed of the spindle has a significant effect on the thermal balance, because of the dependence of the heat generation of the bearings on the spindle speed. And the

higher the rotational speed of the spindle, the shorter it will take to reach the stationary state. According to Fig. 7 (a) and (b), there is a visible short rise of spindle nose temperature as observed in both simulation and experiments, which is produced due to the equalization of higher core temperatures which transfer through the spindle after it is shut off.

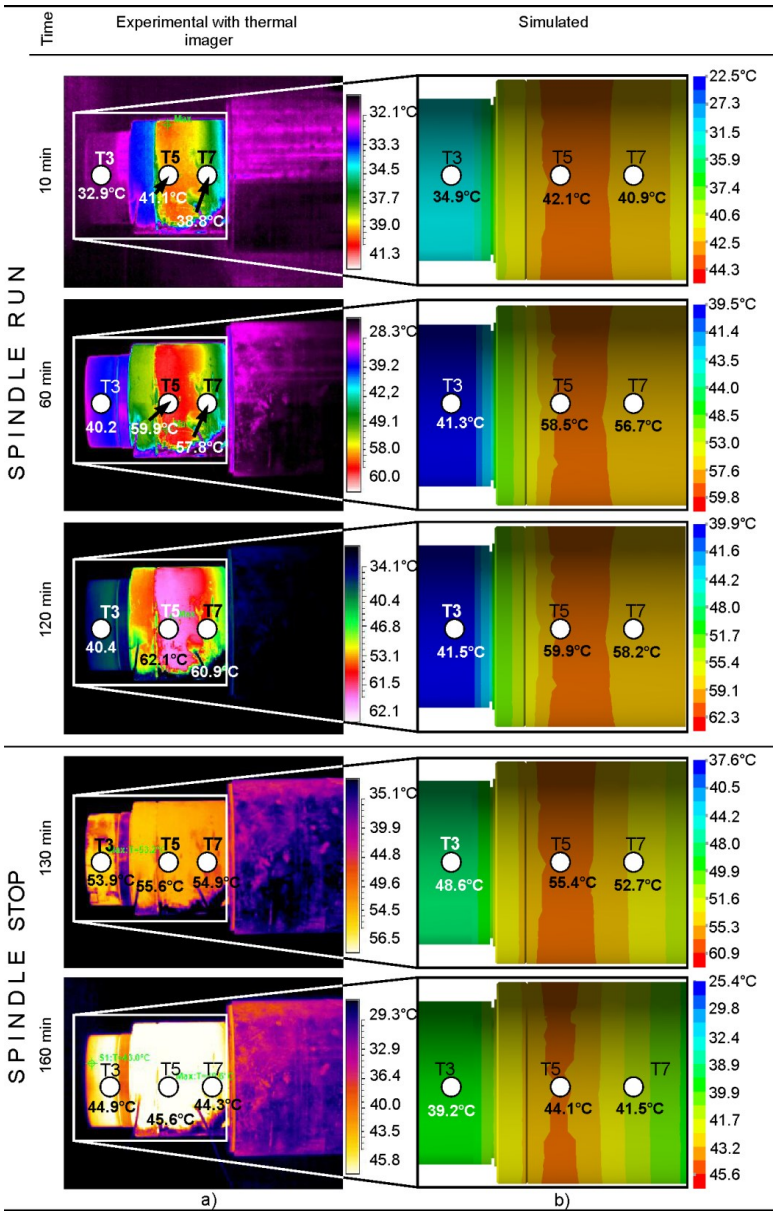

Fig. 7. Comparison of the predicted temperature with the measured value during time.

Thermal displacement. The applied thermal load and the spindle geometry the axial symmetry property cause the symmetry of resultant thermal expansion about the axis of the spindle. Temperatures of the front bearing, housing and spindle shaft near front bearings (Fig. 5a and Fig. 7) are higher than those in the rear, thus the maximal thermal displacement in Y direction occur on the spindle nose, as shown in Figure 8

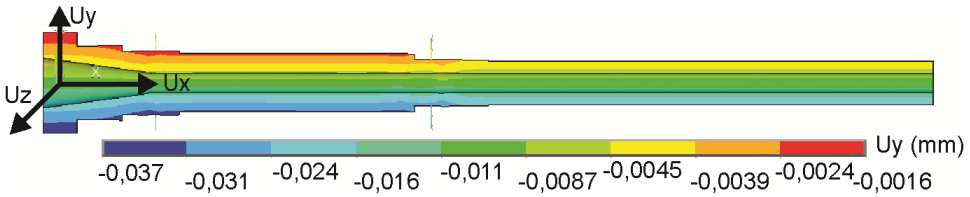

Fig. 8. Thermal displacement of the spindle for 9000 rpm obtained simulated.

The comparison between the measured and simulated thermal displacement of the spindle nose in time and for 9000 rpm is shown in Fiure 8. One of the main causes of this distribution of thermal displacement is the fact that total generated heat is much higher in the front than in the rear bearings. From Figure 9 it can be seen that the Y and Z component of spindle nose are significant than that on X component, which means that the tool displacement in the direction of Y and Z axis will be significant. These displacements can seriously affect the machining precision. On the other hand, in the first time stage, the temperature on the housing increased faster than that of the shaft and more slowly than the temperature on the bearings. Thus, thermal expansion in the spindle shaft is greater than that in the housing leading to a negative thermal expansion u_y between the shaft and housing. This is the reason why both the axial displacement u_x and the preload are increased. In time the spindle shaft's temperature gradient approaches the temperature gradient of the housing. This causes the reduction of negative value u_z, which leads to the decrease of bearing preload during time.

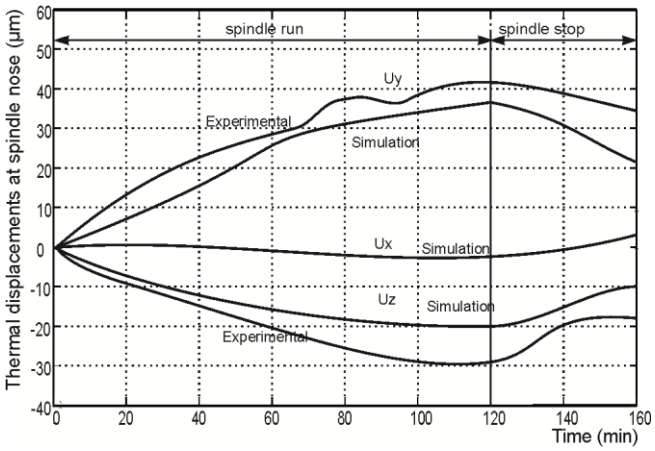

Fig. 9. The thermal displacements in radial direction with time at the spindle nose.

5 Conclusions

A comprehensive method for determining temperature fields and considering a nonlinear thermal-elastic effect on machine tool spindle is presented in this paper. Present model can be separated into two sub-models: the mechanical bearing model and the thermal-elastic model of the spindle shaft. In this paper, the 3D thermal-elastic model of the spindle was created by using the finite element approach. The presented bearing model can be used for non-stationary simulation of the interaction of the internal bearing behavior, and elastic deformation of the spindle. The temperature distribution in the spindle-bearing system was presented and found consistent with experimental results. The distribution of temperature field of the spindle system was characterized according to the simulation results.

Additionally, the simulation errors of the t thermal deformations along the Y and Z axes are less than 11%, which in turn confirms the effectiveness of the simulated model proposed in this paper.

Acknowledgments: In this paper some results of the project: *Contemporary approaches to the development of special solutions related to bearing supports in mechanical engineering and medical prosthetics* – TR 35025, carried out by the Faculty of Technical Sciences, University of Novi Sad, Serbia, are presented. The project is supported by the Ministry of Science and Technological Development of the Republic of Serbia.

References

1. Z. Haitao, Y. Jianguo, S. Jinhua, Int. J. Mach. Tool Manufact., **47** (2007)
2. V.-T. Than, C.-C. Wang, T.-T. Ngo, J.H. Huang, Int. J. Therm. Sci., **111** (2017).
3. J. Mayr, J. et al., CIRP Ann. Manuf. Technol., **61** (2012)
4. W. Wu, X. Li, F. Xu, J. Hong, Y. Li, P. I. Mech. Eng. J-J. Eng., **228** (2014)
5. X. Li, H. Li, J. Hong, Y. Zhang, P. I. Mech. Eng. J-J. Eng., **230** (2016)
6. Y. Zhang, X. Li, J. Hong, K. Yan, S.a. Wang, Adv. Mech. Eng., **8** (2016)
7. 7.T.A. Harris, Michael, N. K., *Rolling bearing analysis: Advanced Concepts of Bearing* (Technology, Taylor & Francis Group, 2007)
8. A. Zivkovic, M. Zeljkovic, S. Tabakovic, Z. Milojevic, Int. J. Adv. Manuf. Technol., **77** (2015)
9. T.A. Harris, Michael, N.K. , *Rolling bearing analysis: Essential Concepts of Bearing* (Technology, Taylor & Francis Group, 2007)
10. B. Bossmanns et al., Int. J. Mach. Tool Manufact., **39** (1999)
11. F.P. Incropera, A.S. Lavine, D.P. DeWitt, *Fundamentals of heat and mass transfer (*John Wiley & Sons, 2011)
12. 12 A. Zivkovic, M. Zeljkovic, C. Mlađenovic, S. Tabakovic, Z. Milojevic, M. Hadzistevic, Thermal Science, DOI: https://doi.org/10.2298/TSCI180129118Z, (2018)